



## Geophysical properties of the crust and upper mantle of the ocean-continent transition in Svalbard area

Marek GRAD<sup>1\*</sup> and Jacek MAJOROWICZ<sup>2</sup>

<sup>1</sup> *Institute of Geophysics, Faculty of Physics, University of Warsaw, ul. Pasteura 5, 02–093 Warszawa, Poland*

<sup>2</sup> *University of Alberta Edmonton, Alberta, Canada – emeritus*

*<majorowi@ualberta.ca>*

*Present Address: 105 Carlson Close, Edmonton AB T6R2J8, Canada*

*\* corresponding author <mgrad@mimuw.edu.pl>*

**Abstract:** This paper presents a review of geophysical studies of the crust and the lithosphere–asthenosphere boundary (LAB) in the ocean–continent transition in the area of Spitsbergen (Svalbard Archipelago) in high Arctic. Over last decades many investigations were performed during Polish geophysical expeditions, as well as in the framework of international cooperation with scientists from Germany, Japan, Norway and USA. We compiled here existing seismic, gravity and thermal models down to LAB depth along the 800 km long transect extending from the actively spreading Knipovich Ridge, across southern Spitsbergen to the Kong Karls Land Volcanic Province. The results of all methods are very consistent, although they are sensitive to different physical parameters: seismic wave velocities, densities and thermal. The thinnest lithosphere of only 12 km is found beneath the Knipovich Ridge. Only 50 km to the west and 50 km to the east of the ridge the LAB depth increases to about 30 km, and this value corresponds to the oceanic structure of the North Atlantic Ocean. Beneath southern Spitsbergen the LAB depth is about 55 km and increases to 90–100 km beneath continental structure of the Barents Sea. The uplift of the LAB close to distance of 700 km along transect could be correlated with Kong Karls Land Volcanic Province.

**Key words:** Arctic, Spitsbergen, Seismic modelling, gravity modelling, thermal modelling, lithosphere–asthenosphere boundary.



## Introduction

The first Polish Arctic expedition was organized during the 2nd Polar Year 1932–1933. Expedition was sent to Bear Island (Bjørnøya) and during 13 months stay the program included a variety of meteorological and geomagnetic studies. Geophysical and geological studies of the Svalbard were continued during 3rd International Geophysical Year 1957–1958. In 1957 Polish scientific station was built at Isbjørnhamna, Hornsund, Southern Spitsbergen (Birkenmajer 1992). This permanent base operates to this day. Over next few decades many of investigations were done by Polish expeditions, as well as, in the framework of international cooperation with scientists from Germany, Japan, Norway and USA (e.g. Mitchell *et al.* 1978; Sellevoll 1982). Extensive geophysical studies in the area of southern Svalbard were performed also during 4th International Polar Year 2007–2008 (e.g. Grad *et al.* 2015).

In this paper we present a compilation of geophysical studies of the crust, lithosphere and the lithosphere-asthenosphere boundary (LAB) along 800 km long transect crossing through the ocean-continent transition in the area of southern Spitsbergen. The transect crosses the Knipovich Ridge in the Northern Atlantic, the continent–ocean boundary (COB), the Hornsund Fault Zone (HFZ), Sørkapp, Storfjorden, Edgeøya and Kong Karls Land Volcanic Province in the western Barents Sea continental platform (Fig. 1, 2). This region has been studied by many geophysical surveys, including active and passive seismic experiments, gravity, magnetic and geothermal investigations (e.g. Vogt *et al.* 1979; Taylor *et al.* 1981; Sellevoll 1982; Davydova *et al.* 1985; Faleide *et al.* 1991; Crane *et al.* 1988, 1991; Dallmann 1999; Klingelhöfer *et al.* 2000a, b; Mjelde *et al.* 2002; Breivik *et al.* 2003; Ljones *et al.* 2004; Czuba *et al.* 2008; Kenyon *et al.* 2008; Maus *et al.* 2009; Grad *et al.* 2015; Klitzke *et al.* 2016).

## Study area

Spitsbergen is the largest, mountainous island of the Svalbard Archipelago and the highest point is Newtontoppen 1713 m a.s.l. Approximately 60% of archipelago is covered by snow and ice. The archipelago is enclosed by seas: the Norwegian Sea, the Greenland Sea, the Barents Sea and the Arctic Ocean (Fig. 1, 2a). Most of the area around Svalbard has a water depth about 250 m (Fig. 2). In the area west of Spitsbergen, in the continental shelf the water depth is increasing to about 2000–2500 m. The deepest parts are in the rift valley of the actively spreading Knipovich Ridge (about 3000 m) and the Molloy Deep (about 4000 m).

The geological succession of the Svalbard Archipelago in general can be divided into three divisions: the ancient basement (Precambrian and Early Palaeozoic), non-metamorphosed sedimentary rocks (Late Palaeozoic to Tertiary), and young, unconsolidated Quaternary sediments (Dallmann 1999).

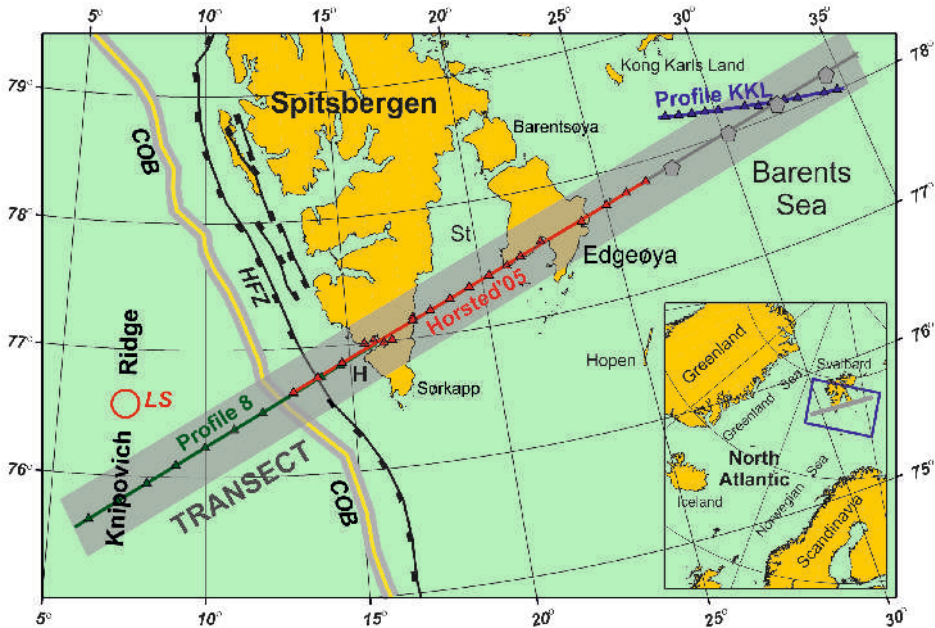
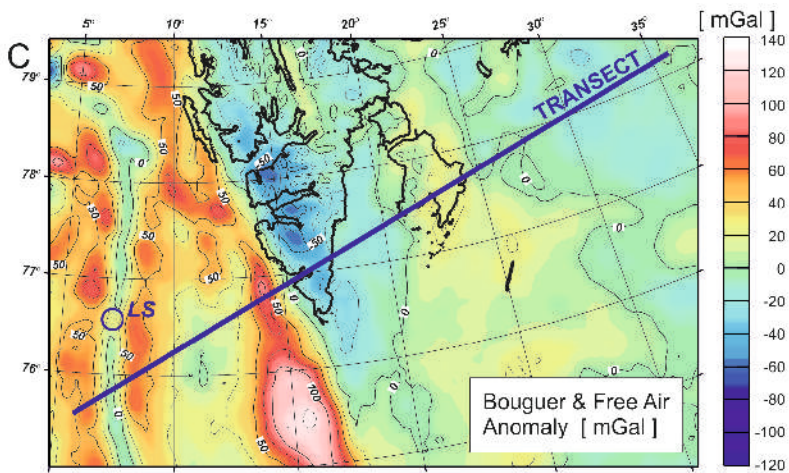
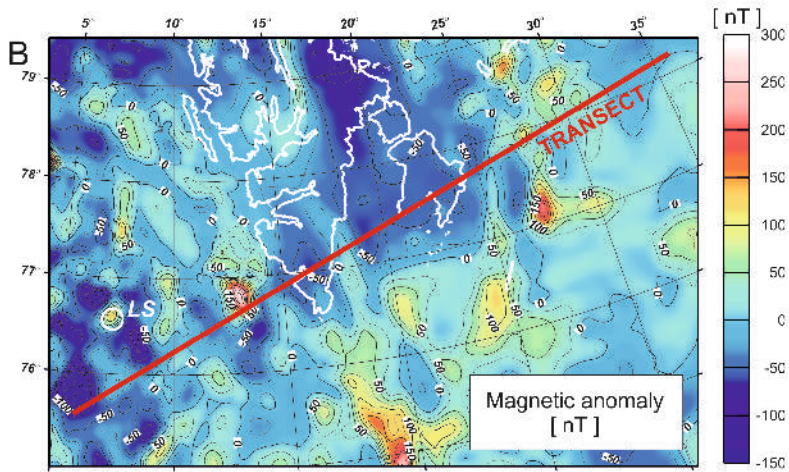
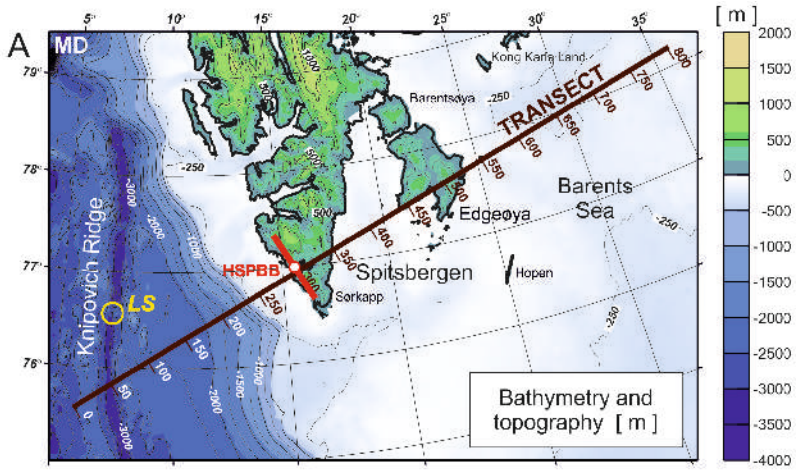


Fig. 1. Location map of the transect in southern Spitsbergen (Svalbard Archipelago), between the Knipovich Ridge and the Barents Sea (highlighted by grey bar). COB – continent–ocean boundary (Breivik *et al.* 1999); H – Hornsund; HFZ – Hornsund Fault Zone; LS – Logachev Seamount; St – Storfjorden. Geographical coordinates of the transect are:  $\varphi_0 = 75.573^\circ\text{N}$ ,  $\lambda_0 = 5.8316^\circ\text{E}$  (0 km of transect in southwest) and  $\varphi_{800} = 78.1909^\circ\text{N}$ ,  $\lambda_{800} = 35.8286^\circ\text{E}$  (800 km of transect, the northeastern-most end). Color lines are seismic profiles: Profile 8 (green), Horsted'05 (red), KKL (deep blue) and data from 3D crustal model of the Barents Sea (grey). Compiled from (Ljones *et al.* 2004; Czuba *et al.* 2008; Minakov *et al.* 2012; Ritzmann *et al.* 2007). Study area is shown in insert.

The crystalline basement of the western Barents Sea is related to the collapse of the Caledonian mountain range (*e.g.* Doré 1991). During Silurian time the Baltica–Laurentia collision was followed by several rifting events. As the rifting stopped, the Barents Shelf subsided as it cooled, and a carbonate platform progressively developed (Worsley 2008). In the Triassic, the sedimentation was dominated by siliciclastic rocks (Riis *et al.* 2008). The second main phase of rifting in the Late Jurassic–Early Cretaceous was related to the northward propagation of the Atlantic (Faleide *et al.* 2008). The relative motion between Svalbard and Greenland during the Mesozoic and Early Cenozoic occurred along the Hornsund Fault Zone (Fig. 1). This regional fault zone can be traced from just south of Bear Island to northern Spitsbergen (Sundvor and Eldholm 1979, 1980) and acted as an incipient plate boundary between the Barents Shelf and the northward propagating Arctic Ocean. The continental breakup of the Arctic occurred at about 53 Ma ago and was accompanied by magmatism on the Norwegian and East Greenland margins (Eldholm *et al.* 2002). No significant separation between Svalbard and Greenland occurred until about 36 Ma ago,



when the relative plate motion between Greenland and Eurasia induced an extensional component along the initially sheared margin segments. Late Cenozoic uplift and glacial erosion has removed most of the Paleogene and Cretaceous succession in the northwestern Barents Sea (Faleide *et al.* 1996). The spreading axis is today represented by the Knipovich Ridge (Fig. 1).

Magmatic intrusions are visible in magnetic anomalies map (Fig. 2b; Maus *et al.* 2009). Magnetic anomalies are mostly from  $-100$  to  $+50$  nT. Positive anomalies over  $+150$  nT are observed west of Hornsund, south of Sørkapp and in the Barents Sea west of Edgeøya. They have circular or elliptic shape with 50 to 100 km diameter. Another group of smaller anomalies occurs in the area of Kong Karls Land (Maus *et al.* 2009; Krysiński *et al.* 2013). Interesting map for the Greenland Sea, Barents Sea and Arctic Ocean shows magnetic anomalies around Spitsbergen (Minakov *et al.* 2012). In the Arctic Ocean symmetrical, regular linear magnetic anomalies are perfectly seen for the Gakkel Ridge, Nansen Basin and Amundsen Basin. On the other hand, nothing of such a pattern is seen in the Greenland Sea, along Knipovich Ridge, where anomalies look rather similar to “random” anomalies in the Barents Sea.

The gravity map of the study area was compiled from free-air anomalies at the sea and Bouguer anomalies on the land with a correction for density of  $2.67 \text{ g/cm}^3$  (Fig. 2c; Kenyon *et al.* 2008; <https://earth-info.nga.mil/GandG/wgs84/agp/readme.html>). The transition from ocean to continent (COB and HFZ) is well seen in that gravity map. The oceanic part is characterized by gravity anomalies from  $+20$  to  $+60$  mGal, with exception of a band of 0 mGal values along the central part of Knipovich Ridge. Anomalies larger than 50 mGal are observed along the whole COB range, with values up to 125 mGal south of Sørkapp. The western Barents Sea is characterized by gravity anomalies from  $-20$  to  $+20$  mGal (Kenyon *et al.* 2008; Krysiński *et al.* 2013).

## Seismicity of the area

Instrumental observations of the seismicity in the European sector of the Arctic region are carried out by a number of seismic services and networks. These include the Norwegian seismological center NOR SAR with a dense seismic network and seismic arrays in Scandinavia and on Svalbard (<http://www.norsardata.no>),

Fig. 2. Transect on the topography/bathymetry map of the study area (A; Jakobsson *et al.* 2000), magnetic map (B; Maus *et al.* 2009) and gravity map (C; Kenyon *et al.* 2008). In the topography/bathymetry map ticks with numbers show distance along transect in km. HSPBB – seismic broadband station which operates in Polish Polar Station Hornsund; LS – Logatchev Seamount; MD – Molloy Deep. Thick red bar shows “fast” polarization of SKS phases which is near parallel to the border between the continental and oceanic crust ( $\alpha = 151.8^\circ$ ). Gravity map is a free-air anomaly at sea and Bouguer anomaly on land with correction for density of  $2.67 \text{ g/cm}^3$  (Kenyon *et al.* 2008).

universities in Bergen and Oslo, and Russian Arkhangelsk seismic network (<http://fciarctic.ru/index.php?page=geoss>). The recent seismicity data of the area are based on NORSTAR and Arkhangelsk seismological networks and were compiled in the unified catalog for 1995–2015 (Antonovskaya *et al.* 2018). The NORSTAR network monitors the area of the Mons and Knipovich ridges and Svalbard, whereas the Arkhangelsk network monitors the area of the Gakkel Ridge, Franz Josef Land, and Novaya Zemlya. The catalog contains seismic events from the European sector of the Arctic ranging from 0.9 to 6.2 in magnitude.

One of the largest intraplate events ever to be instrumentally observed in Arctic was the 21 February 2008 Svalbard earthquake, with magnitude  $M = 5.9$ . It originated by the activation of an oblique-normal fault at a depth of  $15 \pm 5$  km in the lower crust below Storfjorden, just beneath the transect, at distance 400 km (Fig. 3). The main shock initiated a rich aftershock sequence (Pirli *et al.* 2010). The main earthquakes cluster is located along the central axis of the Mid-Atlantic Ridge (Mons, Knipovich and Gakkel ridges). Much weaker seismic activity was

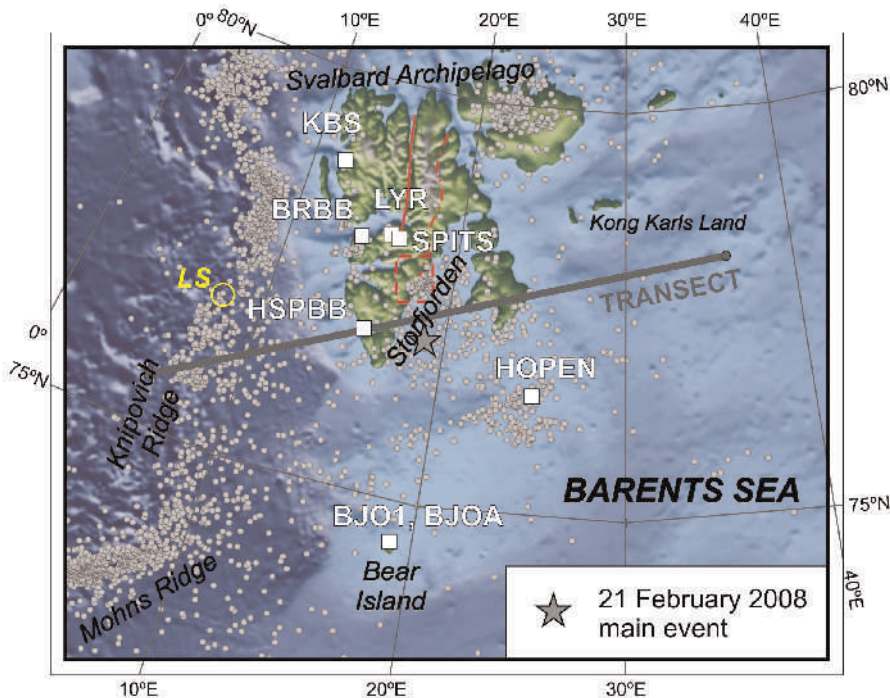


Fig. 3. Transect on the background of seismicity map of Svalbard. Gray circles show locations of epicenters between 1990 and 2007 according to International Seismological Centre (ISC), with epicenter of the 21 February 2008 main event ( $M_w=5.9$ ) indicated with a star. The solid red line on Spitsbergen denotes the Billefjorden fault zone, the dashed red line is Lomfjorden fault, and in their southern termination the dashed red rectangle shows seismic region of Heerland. White squares show locations of seismic stations in the study area. Modified from Pirli *et al.* (2010).

recorded in the Barents Sea and in the Novaya Zemlya fold zone. This seismicity reflects mostly the impact of spreading processes and transform movements.

An interesting pattern of local seismicity was studied in the area of the Logachev Seamount located in the Knipovich Rift valley (Fig. 1 and 2), some 100 km north from the transect (Jokat *et al.* 2012). Observed earthquakes along the Knipovich ridge axis occur there as deep as 25 km. This may be related to cold lithosphere beneath the ultraslow spreading Knipovich Ridge that may lead to brittle behavior potentially down to depths of 25 km below sea-level. However, a prominent zone in the upper mantle underneath Logachev Seamount lacks any earthquakes deeper than 13 km. This depth represents the position of the boundary between brittle and ductile deformation and corresponds to depth of 600°C isotherm. Seismic gap beneath Logachev Seamount can be an indicator for melt process at an ultraslow mid-ocean ridge (Schlindwein *et al.* 2013).

## Seismic models of the crust and upper mantle

A two-dimensional crustal P-wave velocity model along the transect was compiled from several projects (Fig. 4a). In the distance range 0–500 km the model is based on Profile 8 from Ljones *et al.* (2004) and profile Horsted'05 from Czuba *et al.* (2008) and in the distance range 500–800 km the crustal model was constructed on the base of the 2D model along Profile KKL from Minakov *et al.* (2012). The mantle P-wave model is taken from a regional 3D model of the Barents Sea (Levshin *et al.* 2007). The compilation of the crustal and mantle structure down to 250 km depth is shown in Figs. 4b and c (Krysiński *et al.* 2013).

The crustal 2D seismic model (Fig. 4a) documents 6–8 km thick oceanic crust formed at the Knipovich Ridge, a distinct continent–ocean boundary (COB), the eastern boundary of the dominantly sheared Hornsund Fault Zone (HFZ), and the eastern boundary of the Early Cenozoic West Spitsbergen Fold–and–Thrust Belt (WSFTB). The Billefjorden Fault Zone (BFZ) and the main Caledonian suture zone between Laurentia and Barentsia is interpreted based on variations in crustal thickness and velocities (Breivik *et al.* 2003; Krysiński *et al.* 2013). The continental crust beneath the Barents Sea is 28–35 km thick. Teleseismic records of the permanent seismic broadband station HSPBB which operates in the area of the Polish Polar Station Hornsund provided data for receiver function (RF) and SKS phase splitting studies (Wilde-Piórko *et al.* 2009). The results of the RF analysis agree well with structure obtained by refraction seismic studies beneath HSPBB station (Czuba *et al.* 2008), namely south–west dipping basement (at about 7 km depth) and Moho depth of about 32 km.

In the oceanic uppermost mantle P velocities are about 7.85 km/s, while the continental uppermost mantle expresses higher velocities, about 8.25 km/s (Fig. 4b). A zone of decreased velocity may represent the LAB. Below ocean LAB depth is 20–50 km, and 80–100 km beneath the continent. Vertical profiles are shown every

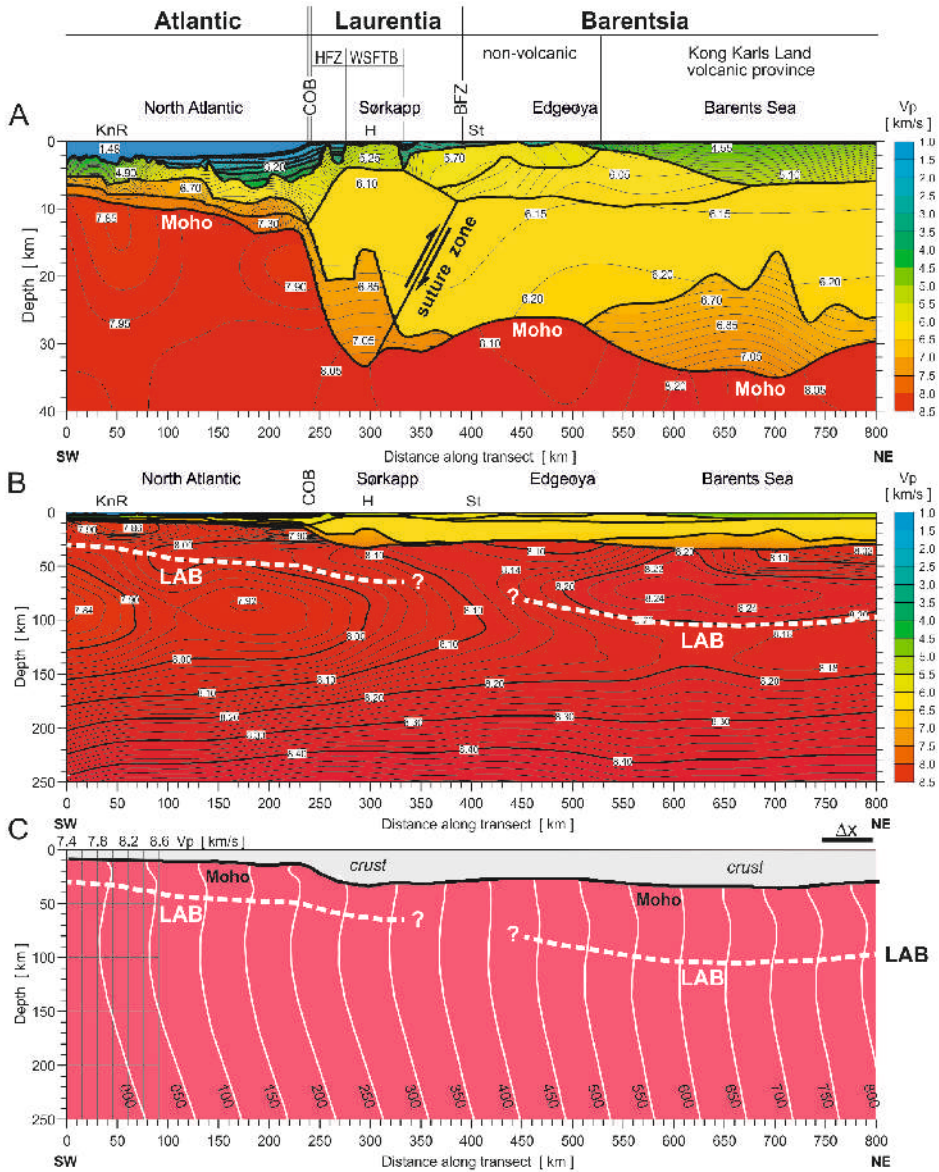


Fig. 4. Seismic P-wave velocity model along the transect. (A) Crustal two-dimensional P-wave velocity model (Ljones *et al.* 2004; Czuba *et al.* 2008; Minakov *et al.* 2012; Krysiński *et al.* 2013). (B) Mantle model down to 250 km compiled from Levshin *et al.* (2007), Czuba *et al.* (2008) and Krysiński *et al.* (2013). (C) One-dimensional P-wave velocity models of the mantle; velocity scale is shown for first curve (000) – next are shifted by  $\Delta x$  corresponding to distance 50 km. H – Hornsund; HFZ – Hornsund Fault Zone; KnR – Knipovich Ridge; LAB – lithosphere-asthenosphere boundary; St – Storfjorden. LAB in the east corresponds to velocity isoline 8.2 km/s at about 100 km depth. In the west it corresponds to velocity isoline 7.96 km/s at about 40 km depth, shallowing to *c.* 20 km below the Knipovich Ridge.

50 km along the transect to better illustrate the low velocity zone (Fig. 4c). Two-dimensional S-wave velocity models of the uppermost mantle along the transect are shown in Fig. 5. The  $V_s$  cross-section was extracted from 3D shear-wave velocity model S2.9EA of the upper mantle beneath Eurasia (Kustowski *et al.* 2008). Velocities down to 250 km depth are shown as  $V_s$  (Fig. 5a) and  $dV_s/V_s$  anomalies (Fig. 5b) in relation to PREM reference model (Dziewonski and Anderson 1981). Lowering  $dV_s/V_s$  in relation to PREM coincides to LAB depth from P-wave velocity and could be identify with isoline  $dV_s/V_s=2.6\%$ . In the continental scale we observe lower velocities beneath ocean (“hot” mantle) and higher velocities beneath continental structures (“cold” mantle). Black dots in Fig. 5b show local seismic events of magnitude  $M$ . We do not observe deeper events than 30–50 km.

Teleseismic records of the HSPBB station provided data for SKS phase splitting which are useful to study mantle anisotropy (Wilde-Piórko *et al.* 2009). Below the Polish Polar Station Hornsund the azimuth of the fast direction of SKS phase is parallel to the continent–ocean boundary with azimuth  $\alpha = 151.8^\circ$  (see red bar in Fig. 2). The average time delay between “fast” and “slow” directions is  $dt = 0.68$  s.

## Crustal and mantle density structure

In addition to seismic modelling, gravity studies were performed for the transect (Krysiński *et al.* 2013; Grad *et al.* 2015). The P-wave seismic velocity model (Fig. 4b) was examined to check whether the velocity model in the crust and mantle can describe isostatic compensation effects observed at the ocean-continent transition. The modelling was performed using the optimization concept (Krysiński *et al.* 2000, 2009; Krysiński 2009). The method postulates construction of some model density distribution  $\rho(x,z)$  using a reference (starting) density-velocity relation  $\rho_{\text{ref}}(v)$ . Constant reference density was assumed in water ( $1.02 \text{ g/cm}^3$ ) and in the mantle ( $3.3 \text{ g/cm}^3$ ). For sediments density-velocity relation was assumed in the form of  $\rho_{\text{ref}}(v)=1.74V^{1/4}$  and for crystalline crust  $\rho_{\text{ref}}(v)=0.328(V-6) + 2.723$ . Divisional analysis made for the crust by Krysiński *et al.* (2009) provides strong constraints for the position and suggested dip of the three main density boundaries along the transect. They were found at distances 240, 280 and 320 km (Fig. 6a), and they represent continent–ocean boundary (COB), Hornsund Fault Zone (HFZ), and eastern boundary of the West Spitsbergen Fold-and-Thrust Belt (WSFTB), respectively.

Gravity-based interpretation (Krysiński *et al.* 2009) divides the crust into relatively high and low-density crustal blocks. The striking and very robustly determined feature of the COB zone is its increased crustal density in relation to the reference velocity-density function (230–270 km in Fig. 6c), which may correspond to mafic/ultramafic or high-grade metamorphic rocks (Gebrande 1982). In the neighboring crustal segment (WSFTB, distance 275–330 km in Fig. 6c),

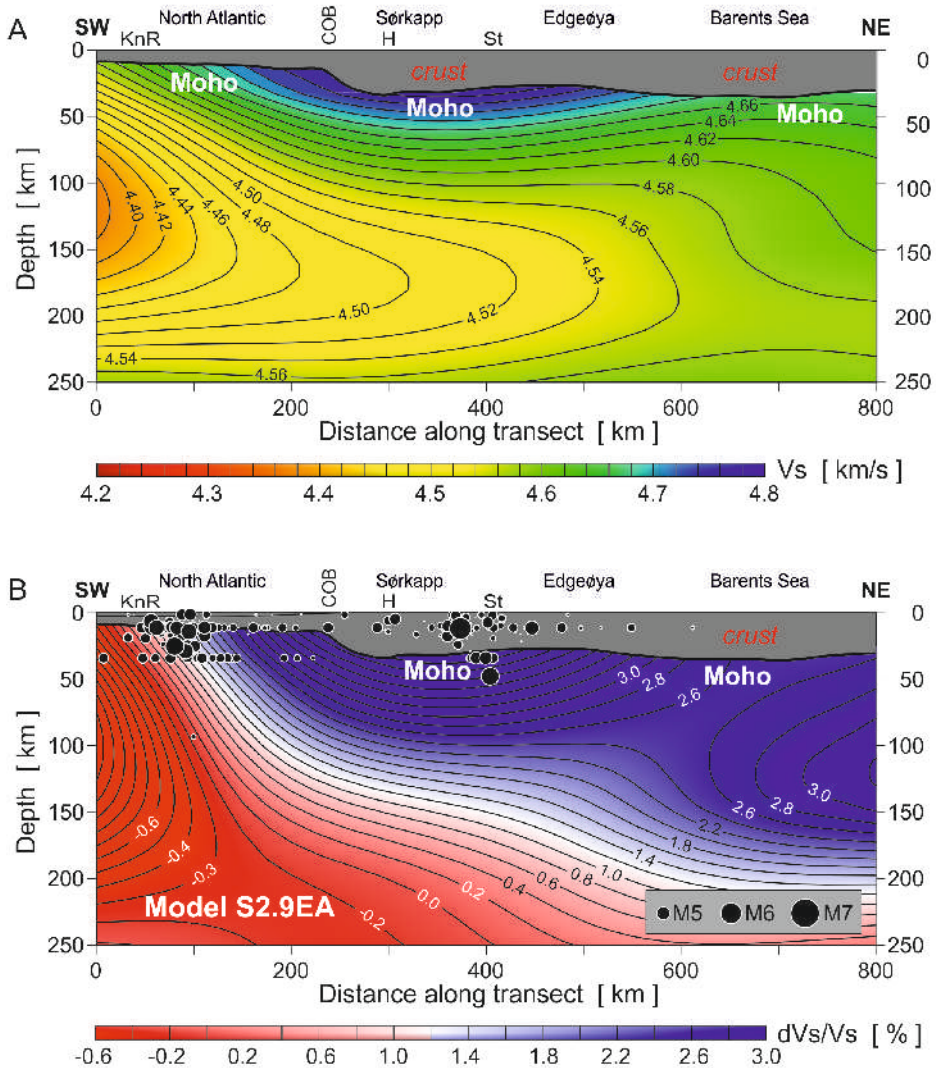


Fig. 5. Regional models of (A) the  $V_s$  and (B)  $dV_s/V_s$  velocity in the mantle down to a depth of 250 km along the transect. Model S2.9EA (Kustowski *et al.* 2008) is compared to PREM reference model (Dziewonski and Anderson 1981). Black dots in figure (B) show local seismic events of magnitude M (after.iris.edu/fdsnws/event/1/).

a distinct deficiency of relative density was found suggesting that the upper-crustal low-velocity massive has probably significantly deeper roots, deeper than 5 km, as indicated in the seismic model (Krysiński *et al.* 2009).

The mantle density–velocity correlation reflects general density difference between the oceanic and continental domains (Krysiński *et al.* 2013). The resulting oceanic mantle density ( $3.15 \text{ g/cm}^3$ ) corresponding to the lowest mantle velocities

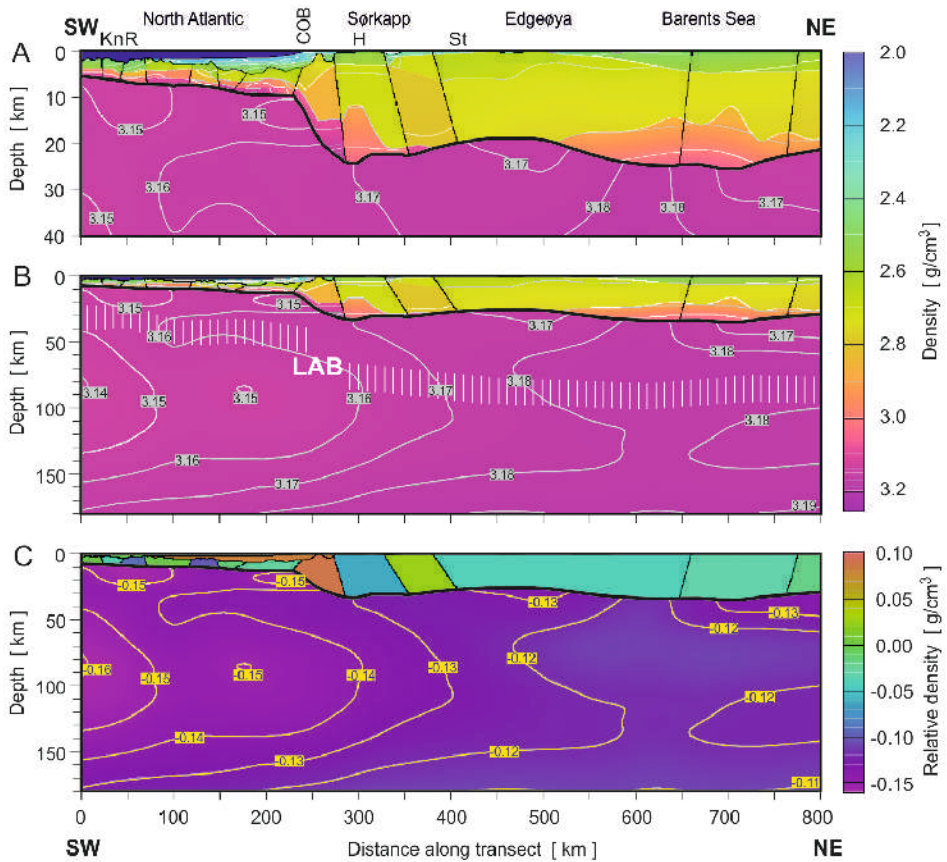


Fig. 6. Density distribution  $\rho(x,z)$  along the transect (Krysiński *et al.* 2013) in the crust (A) and in mantle (B), with relative density shown in (C). White dashed lines in (C) show range of “gravity” LAB.

(7.85 km/s) refers to the uppermost young oceanic mantle (10–30 km depth) which may be interpreted in terms of low heat-flow and composition dominated by dunites. The continental upper mantle expresses high velocities (8.25 km/s) and densities (3.2 g/cm<sup>3</sup>). The “gravity” LAB is not so clear expressed as in velocity model. In oceanic mantle small lowering of density below 3.16 g/cm<sup>3</sup> occurs at depth 30–50 km. In the continental mantle, a small density decrease below 3.18 g/cm<sup>3</sup> occurs at depth 70–100 km. The range of “gravity” LAB is shown in Fig. 6b by white dashed lines.

The results of the gravity modelling show relatively weak correlation of the density with seismic velocity in the upper mantle which suggests that the horizontal differences between oceanic and continental mantle are dominated by mineralogical changes. Significant compositional differences are suggested also by the large range of horizontal velocity variations (Krysiński *et al.* 2013).

## Thermal modelling

Heat flow data in the area of high Arctic are sparse, particularly in comparison to data from continental Europe (e.g. Majorowicz and Wybraniec 2011). For the transect studied here we extracted heat flow data from maps published by Crane *et al.* (1991) and Klitzke *et al.* (2016). Authors of these determinations did not apply paleoclimatic correction. Most of the heat flow data we used come from offshore deep marine conditions. Heat flow probes were lowered to depths where monitored bottom sea temperatures are stable so the paleoclimatic correction was judged to be unnecessary.

Heat flow data in northern Norwegian–Greenland Sea, west of Svalbard, were collected in 80's of the 20th century, from which the contours of observed heat flow were drawn (see fig. 4 in Crane *et al.* 1991). The pattern of surface heat flow is asymmetric across the Knipovich Ridge with the maximum values over  $300 \text{ mW/m}^2$  along the axis of the ridge. Similarly, high values were found also in the Molloy Deep.

More complete coverage of heat flow data over the Barents Sea and Kara Sea have been compiled from multiple publications (see fig. 8a in Klitzke *et al.* (2016)). These data were collected at near-surface depths, so because of paleoclimatic effects or/and groundwater circulation heat flow variations could be beyond a steady-state system. Remember these effects only the main regional trends in surface heat flow variations could be considered. Across the Barents Sea the surface heat flow decreases slightly from west to east, from  $80$  to  $60 \text{ mW/m}^2$ .

Some heat flow data for high Arctic were discussed recently by Antonovskaya *et al.* (2018) and results are similar. In the continental shelf, the average heat flow is about  $70 \text{ mW/m}^2$ . For the oceanic lithosphere with thin crust heat flow increases to  $200 \text{ mW/m}^2$  (Gakkel Ridge) and the maximum value  $484 \text{ mW/m}^2$  was found for northern Knipovich Ridge.

All data mentioned above (Crane *et al.* 1991; Klitzke *et al.* 2016; Antonovskaya *et al.* 2018) used heat flow measurements uncorrected for the paleoclimatic effects. Paleoclimatic correction have been applied across the continental Europe (Majorowicz and Wybraniec 2011). The northern area of Europe was covered by ice sheet during the last glacial maximum, 25–15 ka ago. Corrections are depth dependent due to a diffusive thermal transfer of the surface temperature forcing, of which glacial–interglacial history has the largest impact. Their analysis showed that in shallow cratons and orogenic belts heat flow was underestimated.

Heat flow data extracted from maps along the transect are shown in Fig. 7a. The oceanic areas are characterized by higher heat flow values reaching about  $350 \text{ mW/m}^2$  for the Knipovich Ridge. For the continental area values are close to  $70$ – $80 \text{ mW/m}^2$ . Similar heat flow values above  $70 \text{ mW/m}^2$  were found for the area close to Longyearbyen, some 100 km north from the transect (Midttømme *et al.* 2015; Betlem *et al.* 2018). This compilation of heat flow was used in thermal modelling.

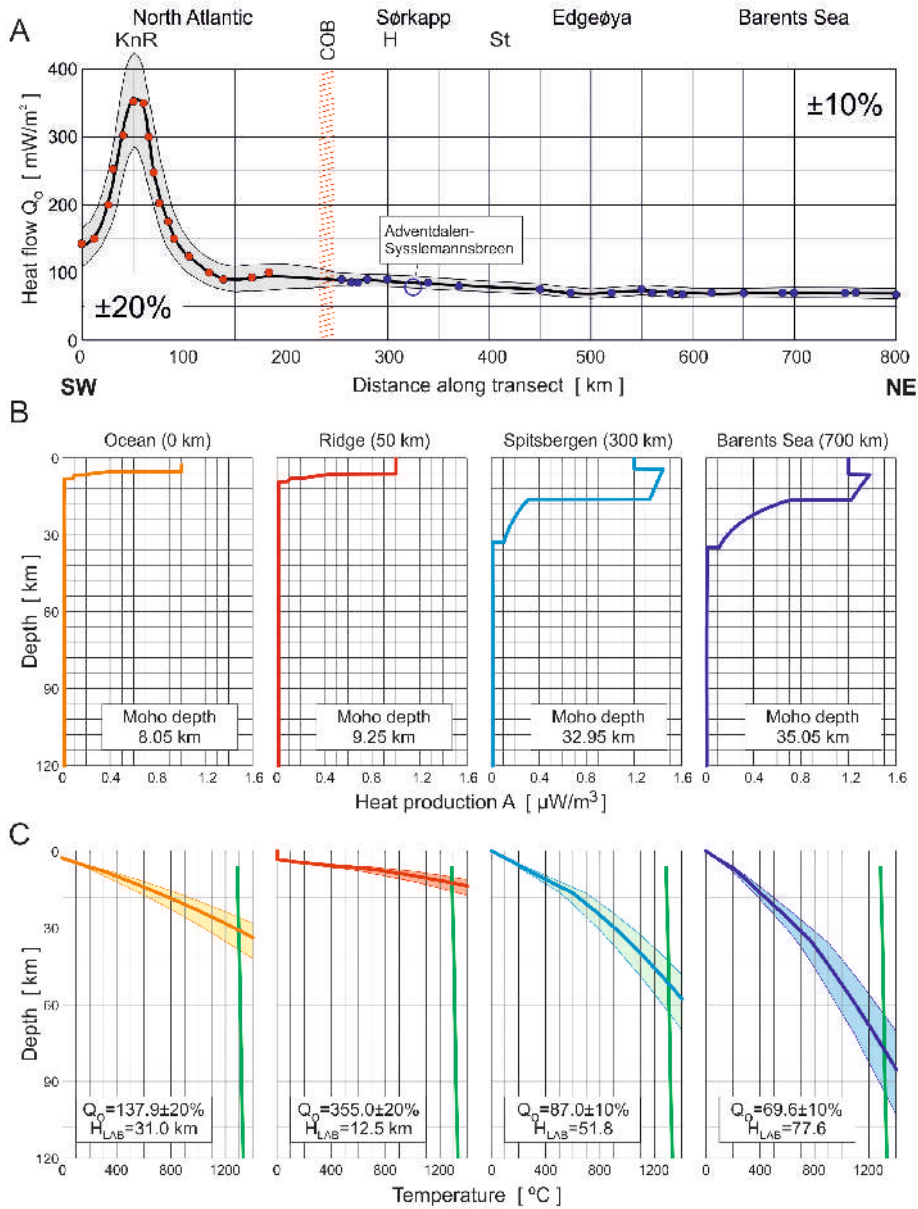


Fig. 7. Heat flow modelling along the transect. (A) Compilation of the heat flow data along the transect from maps: red dots from Crane *et al.* (1991) for oceanic part and navy-blue dots from Klitzke *et al.* (2016) for continental part. Grey band shows range of values  $\pm 20\%$  for ocean and  $\pm 10\%$  for continent (in  $\text{mW/m}^2$ ). COB – continent–ocean boundary (Breivik *et al.* 1999). Open circle at about 325 km of transect indicates a heat flow value above  $70 \text{ mW/m}^2$  for the area of Adventdalen and Sysselmansbreen, close to Longyearbyen, some 100 km north from the transect (Midttømme *et al.* 2015; Betlem *et al.* 2018). (B) Panel shows assumed heat production  $A(z)$  of chosen four sites along transect: for ocean at 0 km of transect, for ridge at 50 km, and for

Due to scarce data distribution calculations were made each 50 km along the transect and examples of thermal modelling are shown in Fig. 7b for chosen four sites along the transect: for oceanic lithosphere at 0 km of the transect, for ridge at 50 km, and for continental crust at 300 km (Spitsbergen) and 700 km (Barents Sea) of transect. Seismic P-wave velocities were extracted from the 2D seismic model along transect (Czuba *et al.* 2008; Grad *et al.* 2015). We assumed surface heat flow  $Q_0 \pm 10\%$  or  $\pm 20\%$  range of this value for continent and ocean, respectively.

The back-stripping of radiogenic heat contribution down to the Moho depth gives mantle heat flow using method described by Hasterok and Chapman (2011). Mantle heat flow  $Q_m$  is calculated from:

$$Q_m = Q_0 - \int A(z_0\text{-Moho}) dz \quad (1)$$

For a one-dimensional steady state case we have used ‘boot strapping’ method described by Hasterok and Chapman (2011)

$$Q_{i+1} = Q_i - A_i dz_i \quad (2)$$

Temperatures  $T_i$  are calculated with:

$$T_{i+1} = T_i + (Q_i/\lambda_i)dz_i - (A_i/2\lambda_i) dz_i^2 \quad (3)$$

Where  $A_i$  and  $\lambda_i$  are intra layers parameters of heat production and rock conductivity changing with depth  $dz_i$ . In addition, thermal conductivity  $\lambda$  of the crust and upper mantle at (P/T) conditions needs to be assumed for the geotherms to be calculated. We used geotherms to determine the thermal LAB. The intersection of our calculated deep geotherms based on paleoclimatic corrected surface heat flow with mantle adiabatic curve from MacKenzie and Canil (1999) gives an estimate of the approximation of thermal LAB depth. In order to calculate geotherm  $T(z)$  as shown in Fig. 7b for the crust and upper mantle down to thermal LAB we take  $dz_i = 1$  km. The enriched peridotite solidus curve runs through 1300°C at some 40 km depth, and 1360°C at 200 km depth

The model of heat production  $A$  (in  $\mu\text{W}/\text{m}^3$ ) with depth  $z$  of the crystalline crust and upper mantle applied along the transect is linked to the 3D seismic velocity  $V_p$

continental crust at 300 km (Spitsbergen) and 700 km (Barents Sea) of transect (C). Thermal characteristic of chosen four sites along transect. For seismic P-wave velocity model of the crust extracted from the 2D seismic model along transect (Czuba *et al.* 2008; Grad *et al.* 2015), surface heat flow  $Q_0$  and assumed models of heat production  $A$  and conductivity  $\lambda$  with depth  $z$ . See Table 1 and text for detailed description. Thick color lines in diagrams show temperature distribution (geotherms) with depth, for surface heat flow  $Q_0$  and  $\pm 10\%$  or  $\pm 20\%$  of this value. The thick green lines show enriched peridotite solidus (MacKenzie and Canil 1999; Hirschmann 2000). Their intersects with geotherms give thermal LAB depths.

model and similar to the modelling done in Majorowicz *et al.* (2019 a, b). It is based on the lab derived empirical  $A(V_p)$  relationship (*e.g.* Rybach 1978; Rybach and Buntebarth 1984) farther adjusted for in situ temperature-depth in situ conditions by Čermák and Bodri (1986a, b). The  $A$  for the sediments was assumed to be in the 1.0–1.2 ( $\mu\text{W}/\text{m}^3$ ) range with lesser number assumed for the oceanic younger sediments and higher for the continental part. The lowermost part belonging to the mantle production was estimated to 0.01 ( $\mu\text{W}/\text{m}^3$ ) as in Balling (1995) and Correia and Safanda (2002).

Moho heat flow  $Q_m$  was calculated using equations (1) and (2). Calculations of  $Q_m$  were made each 50 km along transect for ocean at 0 km and 100 km ( $Q_m = 125\text{--}135 \text{ mW}/\text{m}^2$ ) in the vicinity of the rift at 50 km ( $Q_m = 350 \text{ mW}/\text{m}^2$ ) and in the oceanic section west of COB at 150 km and 200 km ( $Q_m = 85 \text{ mW}/\text{m}^2$ ). In the transition between the ocean and continent at 250 km  $Q_m = 70 \text{ mW}/\text{m}^2$ . Much lower  $Q_m = 60 \text{ mW}/\text{m}^2$  characterize continental crust at 300 km at Spitsbergen and  $Q_m = 35\text{--}40 \text{ mW}/\text{m}^2$  at the the Barents Sea section of the transect.

Table 1.

Heat flow values and depths of main seismic boundaries along transect.

Distance along transect [km]	Heat flow [ $\text{mW}/\text{m}^2$ ]	Water depth [km]	Depth of basement [km]	Depth of the upper crust floor [km]	Depth of the lower crust floor [km]	Moho depth [km]
0	137.9	2.75	5.35	6.45	7.95	8.05
50	355.0	3.25	6.15	7.75	9.15	9.25
100	129.5	2.25	5.65	8.25	10.15	10.25
150	89.7	2.15	5.35	9.65	10.95	11.05
200	93.6	1.85	8.25	10.85	13.45	13.55
250	88.8	0.05	9.55	17.45	23.25	23.35
300	87.0	0.05	4.15	16.15	32.85	32.95
350	82.7	–	5.75	28.55	31.15	31.25
400	78.6	0.05	0.75	27.65	–	27.75
450	74.4	–	0.25	26.05	–	26.15
500	68.6	–	0.15	26.45	–	26.55
550	72.6	–	1.55	24.15	30.85	30.95
600	69.5	0.05	3.25	23.25	33.65	33.75
650	69.2	0.15	5.85	20.25	33.75	33.85
700	69.6	0.15	6.35	16.35	34.95	35.05
750	69.1	0.15	6.15	24.85	31.65	31.75
800	69.0	0.15	5.85	25.95	29.55	29.65

Crustal radiogenic heat flow contribution:

$$Q_c = \int A(z_0\text{-Moho}) dz \quad (4)$$

in oceanic crust is in single digits (3–9 mW/m<sup>2</sup>). In the continental crust it varies at typical crustal values 30–40 mW/m<sup>2</sup>. High input of heat from the mantle characterizing the rift and young oceanic part at very low contribution of heat from the crustal part is typical for transient heat contribution in young generated oceanic crust (Lucazeau 2019).

The model of thermal conductivity  $\lambda$  (in W/m°C) assumes  $\lambda = 2.4$  for sedimentary rocks,  $\lambda = 3.0$  for the upper crust,  $\lambda = 2.7$  for the middle crust,  $\lambda = 2.3$  for the lower crust and  $\lambda = 2.5$  for the upper mantle (Balling 1995; Čermák and Bodri 1986a, b; Correia and Safanda 2002) for which a temperature-depth correction was applied after Chapman and Furlong (1992). This results in decrease of conductivity with temperature increase in the upper crustal rocks and increase of conductivity with depth in the mantle (Čermák and Bodri 1986b). Geotherms were calculated with five iterations; first iteration with  $\lambda(z)$  not depended on temperature/pressure (ambient conditions) and next four iterations with  $\lambda(z)$  depended on  $T(z)$ , according to Chapman and Furlong (1992). We observed that last fifth iteration shows no significant changes comparing to iteration four, so this geotherm was used to determine temperature-depth and used in the determination of the LAB depth (Fig. 7b, 8). Thick color lines in Fig. 7b show temperature distribution (geotherms) with depth, and their intersections

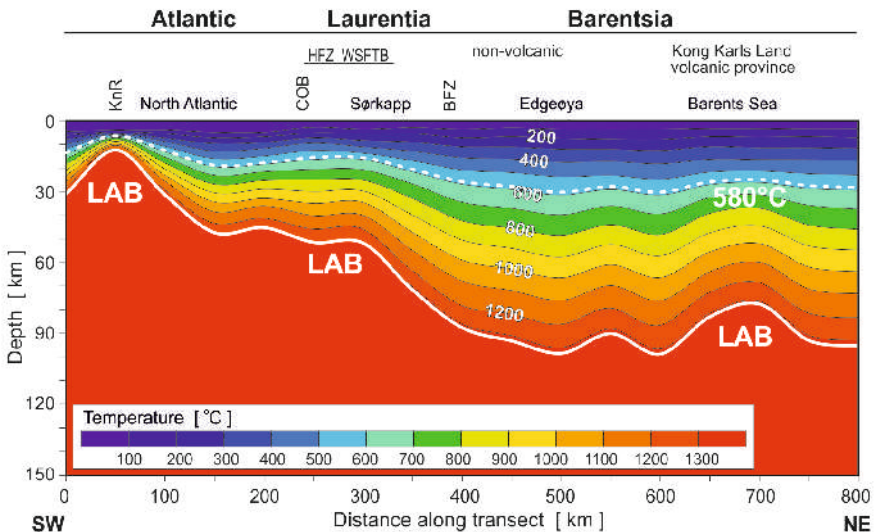


Fig. 8. Temperature distribution along the transect. Smooth section for calculations made each 50 km along transect. Thick dashed white line – isoline of 580°C (Curie temperature).

with enriched peridotite solidus (MacKenzie and Canil 1999; Hirschmann 2000) give the thermal LAB depths. Influence of  $\pm 10\%$  /  $\pm 20\%$  assumed error of heat flow upon the LAB depth is shown and varies depending on the position/depth of LAB. It reaches up to  $\pm 14$  km, however, uncertainties in the models of  $A$  and  $\lambda$  may be causing similar errors (Čermák and Bodri 1986b).

## Complex geophysical model along the transect

The structure of the crust and the lithosphere-asthenosphere system in the ocean-continent transition along the transect extending from the actively spreading Knipovich Ridge, across southern Spitsbergen to the Kong Karls Land Volcanic Province was investigated using seismic, gravity and thermal methods. Their summary is compiled in Fig. 9, particularly showing crust with seismic Moho depth, seismic LAB, and depth of temperature  $580^\circ\text{C}$  (Curie temperature) and thermal LAB depth, both determined from thermal studies.

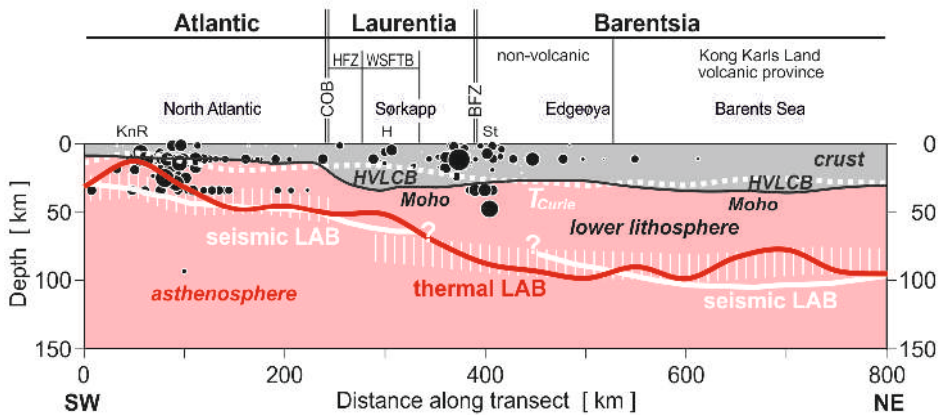


Fig. 9. Cartoon with summary of the crust and lithosphere-asthenosphere beneath transect from seismic, gravity and heat flow investigations. Thick dashed white line shows depth of temperature  $580^\circ\text{C}$  (Curie temperature), white solid lines show seismic LAB (compare Fig. 4b, c) and red line shows thermal LAB (compare Fig. 8). HVLCB – high velocity lower crustal bodies. Black dots show local seismic events (compare Fig. 5).

Oceanic crust formed at the Knipovich Ridge extends from the western end of the transect and COB. Sedimentary cover up to 5 km thick overlay the three-layered magmatic crust for which the total thickness of the magmatic crust is about 6–8 km. East of the COB, the continental crust up to 35 km thick extends to the end of transect. In two regions, in the distance range 250–350 km and 550–800 km, high velocity lower crustal bodies (HVLCB) were found with P-wave velocities  $>7$  km/s. These bodies of relatively low heat production

A have a significant influence upon crustal heat flow, and consequently on the temperature distribution. The calculated depth of isotherm 580°C (identify as Curie temperature) roughly follows the depth of oceanic and continental Moho. Exceptions are high velocity bodies where it follows top of HVLCB (Czuba *et al.* 2008). Knowledge of Curie isotherm has crucial importance for modelling of magnetic properties of the crust. In places where HVLCB are present, the Curie depth tends to follow the top of these structures.

The oceanic upper mantle is characterized by relatively low density 3.15 g/cm<sup>3</sup>) corresponding to the lowest mantle velocities 7.86–8.0 km/s and refers to the uppermost young oceanic mantle at 10–30 km depth. Such velocities and densities in the oceanic lithosphere suggest composition dominated by primitive peridotites. In contrast, the continental upper mantle expresses high velocities (8.24 km/s) and densities (3.2 g/cm<sup>3</sup>), which may be interpreted as composition dominated by dunites.

Results of all methods for LAB determination are generally consistent, despite they use different parameters: seismic wave velocities, densities and geothermal. The lithosphere is the thinnest beneath The Knipovich Ridge, particularly beneath central rift valley, being 12 km only. The Knipovich Ridge which is a part of the Mid-Atlantic Ridge system can be traced in the northern Greenland Sea as a well-developed, ultra-slow spreading ridge (Jokat *et al.* 2012; Schlindwein *et al.* 2013). Only 50 km to the west and 50 km east of the LAB depth increases to about 30 km, and this value corresponds to oceanic structure of North Atlantic and it follows a reference cooling model. Toward the COB (continent–ocean boundary) the LAB depth increases to about 50 km. West of Hornsund the COB is narrow, only about 20 km wide. This transition extends from clear oceanic crust ( $V_p=6.7\text{--}7.3$  km/s) to continental crust with significantly lower velocities (about  $V_p=6.1$  km/s) and Moho depths about 10 km and about 30 km, respectively. Beneath southern Spitsbergen the LAB depth is about 55 km and increases to 90–100 km beneath continental structure of the Barents Sea. Small uplifts of LAB close to distance of 300 km and 700 km could be correlated with high velocity lower crustal bodies (HVLCB) in the lower crust. However, these bodies of relatively low heat production A (high  $V_p$  and low A) have a significant influence on the calculation of crustal-mantle heat flow, and consequently on the higher temperatures in the crust. At 700 km  $Q_m$  is calculated to be elevated at 43 mW/m<sup>2</sup>, some 6–9 mW/m<sup>2</sup> higher than in surrounding  $\pm 50$  km to the east and west.

Earthquakes are concentrated beneath Knipovich Ridge and below Stor-fjorden, just beneath the transect, at distance 400 km (Fig. 3 and Fig. 5). All events occur in “cold” lithosphere. We do not observe deeper events than 30–50 km, none are in the asthenosphere.

**Acknowledgements.** – This work was partially supported by NCN grant DEC-2011/02/A/ST10/00284. The authors thanks Professor Miroslav Bielik and an anonymous reviewer for their comments, which have led to an improved revised manuscript. Second

author, JAM thanks his former employer Department of Physics, University of Alberta for general support. The public domain GMT software (Wessel and Smith 1991, 1998) has been used for plotting maps.

## References

- ANTONOVSKAYA G.N., BASAKINA I.M. and KONECHNAYA YA.V. 2018. Distribution of Seismicity and Heat Flow Anomalies in the Barents Sea Region. *Geotectonics* 52: 45–55.
- BALLING N. 1995. Heat flow and thermal structure of the lithosphere across the Baltic Shield and northern Tornquist Zone. *Tectonophysics* 244: 13–50.
- BETLEM P., MIDTTØME K., JOCHMANN M., SENGER K. and OLAUSSEN S. 2018. Geothermal gradients on Svalbard, Arctic Norway. First EAGE/IGA/DGMK Joint Workshop on Deep Geothermal Energy. doi: 10.3997/2214-4609.201802945.
- BIRKENMAJER K. 1992. Polish geological investigations in Svalbard. *Earth Sciences History* 11: 81–87.
- BREVIK A.J., VERHOEF J. and FALÉIDE J.I. 1999. Effect of thermal contrasts on gravity modeling at passive margins: results from the western Barents Sea. *Journal of Geophysical Research* 104: 15293–15311.
- BREVIK A.J., MJELDE R., GROGAN P., SHIMAMURA H., MURAI Y. and NISHIMURA Y. 2003. Crustal structure and transform margin development south of Svalbard based on ocean bottom seismometer data. *Tectonophysics* 369: 37–70.
- CHAPMAN D.S. and FURLONG K.P. 1992. Thermal state of the continental lower crust. In: D.M. Fountain, R. Arculus and R.W. Kay (eds), *Continental lower crust*. Elsevier, Amsterdam, pp 179–199.
- ČERMÁK V. and BODRI L. 1986a. Temperature structure of the lithosphere based on 2D temperature modelling, applied to central and eastern Europe. In: J. Burrus (ed.), *Thermal modeling in sedimentary basins: 1st IFP Exploration Research Conference, Carcans, France, June 3–7, 1985. Collection Colloques Et Seminaires, 44, Imprint Paris, pp 7–31 (Editions Technip)*.
- ČERMÁK V. and BODRI L. 1986b. Two-dimensional temperature modelling along five east European geotraverses. *Journal of Geodynamics* 5: 133–163.
- CORREIA A. and SAFANDA J. 2002. Geothermal modelling along a two-dimensional crustal profile in Southern Portugal. *Journal of Geodynamics* 34: 47–61.
- CRANE K., SUNDVOR E., FOUCHER J.P., HOBART M., MYHRE A.M. and LEDOURAN S. 1988. Thermal Evolution of the Western Svalbard Margin. *Marine Geophysical Research* 9: 165–194.
- CRANE K., SUNDVOR E., BUCK R. and MARTINEZ F. 1991. Rifting in the Northern Norwegian-Greenland Sea: thermal tests of asymmetric spreading. *Journal of Geophysical Research* 96: 14529–14550.
- CZUBA W., GRAD M., GUTERCH A., MAJDAŃSKI M., MALINOWSKI M., MJELDE R., MOSKALIK M., ŚRODA P., WILDE-PIÓRKO M. and NISHIMURA Y. 2008. Seismic crustal structure along the deep transect Horsted’05, Svalbard. *Polish Polar Research* 29: 279–290.
- DALLMANN W.K. (ed.) 1999. *Lithostratigraphic Lexicon of Svalbard*. Norwegian Polar Institute, Tromsø: 318 pp.
- DAVYDOVA N.I., PAVLENKOVA N.I., TULINA YU.V. and ZVEREV S.M. 1985. Crustal structure of the Barents Sea from seismic data. *Tectonophysics* 114: 213–231.
- DORÉ A.G. 1991. The structural foundation and evolution of Mesozoic seaways between Europe and the Arctic. *Palaeogeography, Palaeoclimatology, Palaeoecology* 87: 441–492.
- DZIEWONSKI A.M. and ANDERSON D.L. 1981. Preliminary reference Earth model. *Physics of the Earth and Planetary Interiors* 25: 297–356.
- ELDHOLM O., TSIKALAS F. and FALÉIDE J.I. 2002. The continental margin off Norway 62–75°N: Palaeogene tectono-magmatic segmentation and sedimentation. In: D.W. Jolley and B.R. Bell

- (eds.) The North Atlantic Igneous Province: Stratigraphy, Tectonics, Volcanic and Magmatic Processes. *Geological Society, London, Special Publications* 197: 39–68.
- FALEIDE J.I., GUDLAUGSSON S.T., ELDHOLM O., MYHRE A.M. and JACKSON H.R. 1991. Deep seismic transects across the sheared western Barents Sea–Svalbard continental margin. *Tectonophysics* 189: 73–89.
- FALEIDE J.I., SOLHEIM A., FIEDLER A., HJELSTUEN B.O., ANDERSEN E.S. and VANNESTE K. 1996. Late Cenozoic evolution of the western Barents Sea–Svalbard continental margin. *Global and Planetary Change* 12: 53–74.
- FALEIDE J.I., TSICALAS F., BREIVIK A.J., MJELDE R., RITZMANN O., ENGEN Ø., WILSON J. and ELDHOLM O. 2008. Structure and evolution of the continental margin off Norway and the Barents Sea. *Episodes* 31: 82–91.
- GEBRANDE H. 1982. Elastic wave velocities and constants of elasticity of rocks and rock forming minerals. In: G. Angenheister (ed.) *Landolt–Börnstein, Physical Properties of Rocks, Band V/1b*. Springer Verlag, Berlin, Heidelberg: 1–99.
- GRAD M., MJELDE R., KRYSIŃSKI L., CZUBA W., LIBAK A., GUTERCH A. and IPY PROJECT GROUP 2015. Geophysical investigations of the area between the Mid-Atlantic Ridge and the Barents Sea: from water to the lithosphere–asthenosphere system. *Polar Science* 9: 168–183.
- HASTEROK D. and CHAPMAN D.S. 2011. Heat production and geotherms for the continental lithosphere. *Earth and Planetary Science Letters* 30: 59–70.
- HIRSCHMANN M.M. 2000. Mantle solidus: experimental constraints and the effects of peridotite composition. *Geochemistry, Geophysics, Geosystems* 1: 2000GC000070.
- JAKOBSSON M., CHERKIS N.Z., WOODMARD J., MACNAB R. and COAKLEY B. 2000. New grid of Arctic bathymetry aids scientists and mapmakers. *EOS, Transaction, American Geophysical Union* 81: 89, 93, 96.
- JOKAT W., KOLLOFRATH J., GEISSLER W.H. and JENSEN L. 2012. Crustal thickness and earthquake distribution south of the Logachev Seamount, Knipovich Ridge. *Geophysical Research Letters* 39: L08302.
- KENYON S., FORSBERG R. and COAKLEY B. 2008. New Gravity Field for the Arctic. *EOS, Transaction, American Geophysical Union* 89: 289.
- KLITZKE P., SIPPEL J., FALEIDE J.I. and SCHECK-WENDEROTH M. 2016. A 3D gravity and thermal model for the Barents Sea and Kara Sea. *Tectonophysics* 684: 131–147.
- KLINGELHÖFER F., GÉLI L. L. and WHITE R.S. 2000a. Geophysical and geochemical constraints on crustal accretion at the very–slow spreading Mohns Ridge. *Geophysical Research Letters* 27: 1547–1550.
- KLINGELHÖFER F., GÉLI L., MATIAS L., STEINSLAND N. and MOHR J. 2000b. Crustal structure of a super–slow spreading centre: a seismic refraction study of Mohns Ridge, 72°N. *Geophysical Journal International* 141: 509–526.
- KRYSIŃSKI L., GRAD M. and POLONAISE WORKING GROUP 2000. POLONAISE’97–Seismic and gravimetric modelling of the crustal structure in the Polish basin. *Physics and Chemistry of the Earth, Part A* 25: 355–363.
- KRYSIŃSKI L. 2009. Systematic methodology for velocity–dependent gravity modelling of density crustal cross–sections, using an optimization procedure. *Pure and Applied Geophysics* 166: 375–408.
- KRYSIŃSKI L., GRAD M. and WYBRANIEC S. 2009. Searching for regional crustal velocity–density relations with the use of 2–D gravity modelling – Central Europe case. *Pure and Applied Geophysics* 166: 1913–1936.
- KRYSIŃSKI L., GRAD M., MJELDE R., CZUBA W. and GUTERCH A. 2013. Seismic and density structure of the lithosphere–asthenosphere system along transect Knipovich Ridge–Spitsbergen–Barents Sea – geological and petrophysical implications. *Polish Polar Research* 34: 111–138.
- KUSTOWSKI B., EKSTRÖM G. and DZIEWOŃSKI I A. 2008. The shear-wave velocity structure in the upper mantle beneath Eurasia. *Geophysical Journal International* 174: 978–992.

- LEVSHIN A.L., SCHWEITZER J., WEIDLE C., SHAPIRO N.M. and RITZWOLLER M.H. 2007. Surface wave tomography of the Barents Sea and surrounding regions. *Geophysical Journal International* 170: 441–459.
- LJONES F., KUWANO A., MJELDE R., BREIVIK A., SHIMAMURA H., MURAI Y. and NISHIMURA Y. 2004. Crustal transect from the North Atlantic Knipovich Ridge to the Svalbard Margin west of Hornsund. *Tectonophysics* 378: 17–41.
- LUCAZEAU F. 2019. Analysis and mapping of an updated terrestrial heat flow data set. *Geochemistry, Geophysics, Geosystems*, 20: 4001–4024.
- MACKENZIE J.M. and CANIL D. 1999. Composition and thermal evolution of cratonic mantle beneath the central Archean Slave Province, NWT, Canada. *Contributions to Mineralogy and Petrology* 134: 313–324.
- MAJORIWICZ J. and WYBRANIEC S. 2011. New terrestrial heat flow map of Europe after regional paleoclimatic correction application. *International Journal of Earth Sciences* 100: 881–887.
- MAJOROWICZ J., GRAD M. and POLKOWSKI M. 2019a. Terrestrial heat flow versus crustal thickness and topography – European continental study. *International Journal of Terrestrial Heat Flow and Applied Geothermics* 2: 17–21.
- MAJOROWICZ J., POLKOWSKI M. and GRAD M. 2019b. Thermal properties of the crust and the lithosphere-asthenosphere boundary in the area of Poland from the heat flow variability. *International Journal of Earth Sciences* 108: 649–672.
- MAUS S., BARCKHAUSEN U., BERKENBOSCH H., BOURNAS N., BROZENA J., CHILDERS V., DOSTALER F., FAIRHEAD J.D., FINN C., VON FRESE R.R.B., FAINA C., GOLYNSKY S., KUCKS R., LUHR H., MILLIGAN P., MOGREN S., MULLER D., OLESEN O., PILKINGTON M., SALTUS R., SCHRECKENBERGER B., THEBAULT E. and CARATORI TONTINI F. 2009. EMAG2: A 2-arc-minute resolution Earth Magnetic Anomaly Grid compiled from satellite, airborne and marine magnetic measurements. *Geochemistry, Geophysics, Geosystem* 10: Q08005.
- MIDTØMME K., JOHMAN M., HENNE I., THOMAS P. and WANGEN M. 2015. Is geothermal energy an alternative for Svalbard? Research Gate, <https://www.researchgate.net/publication/281465492>.
- MITCHELL B.J., VINCEZ S.A., DUDA S., TEISSEYRE R., GUTERCH A. and SELLEVOLL M.A. 1978. Geophysical research on Spitsbergen. *Arctic Bulletin* 2: 314–319.
- MINAKOV A., MJELDE R., FALEIDE J.I., FLUEH E.R., DANNOWSKI A. and KEERS H. 2012. Mafic intrusions east of Svalbard imaged by active-source seismic tomography. *Tectonophysics* 518–521: 106–118.
- MJELDE R., BREIVIK A.J., ELSTAD H., RYSETH A.E., SKILBREI J.R., OPSAL J.G., SHIMAMURA H., MURAI Y. and NISHIMURA Y. 2002. Geological development of the Sørvestsnaget Basin, SW Barents Sea, from ocean bottom seismic, surface seismic and potential field data. *Norwegian Journal of Geology* 82: 183–202.
- PIRLI M., SCHWEITZER J., OTTEMÖLLER L., RAFESI M., MJELDE R., ATAKAN K., GUTERCH A., GIBBSON S.J., PAULSEN B., DĘBSKI W., WIEJACH P. and KVÆRNA T. 2010. Preliminary analysis of the 21 February 2008 Svalbard (Norway) seismic sequence. *Seismological Research Letters* 81: 63–75.
- RIIS F., LUNDSCHIEN B.A., HØY T., MØRK A. and MØRK M.B.E. 2008. Evolution of the Triassic shelf in the northern Barents Sea region. *Polar Research* 27: 318–338.
- RYBACH L. 1978 The relationship between seismic velocity and radioactive heat production in crustal rocks: an exponential law. *Pure and Applied Geophysics* 117: 75–82.
- RYBACH L. and BUNTEBARTH G. 1984. The variation of heat generation density and seismic velocity with rock type in the continental crust. *Tectonophysics* 103: 309–344.
- SCHLINDWEIN V., DEMUTH A., GEISSLER W.H. and JOKAT W. 2013. Seismic gap beneath Logachev Seamount: Indicator for melt focusing at an ultraslow mid-ocean ridge? *Geophysical Research Letters* 40: 1703–1707.
- SELLEVOLL M.A. (ed.) 1982. *Seismic crustal studies on Spitsbergen 1978*. Geophysical Research on Spitsbergen, Bergen: 62 pp.

- SUNDEVOR E. and ELDHOLM O. 1979. The western and northern margin off Svalbard. *Tectonophysics* 59: 239–250.
- SUNDEVOR E. and ELDHOLM O. 1980. The continental margin of the Norwegian–Greenland Sea: Recent and outstanding problems. *Transactions of the Royal Society of London Series A* 294: 77–82.
- TAYLOR P.T., KOVACS L.C., VOGT P.R. and JOHNSON G.L. 1981. Detailed aeromagnetic investigation of the Arctic Basin, 2. *Journal of Geophysical Research* 86: 6323–6333.
- VOGT P.R., TAYLOR P.T., KOVACS L.C. and JOHNSON G.L. 1979. Detailed aeromagnetic investigation of the Arctic Basin. *Journal of Geophysical Research* 84: 1071–1089.
- WESSEL P. and SMITH W.H.F. 1991. Free software helps map and display data. *EOS, Transaction, American Geophysical Union* 72: 445–446.
- WESSEL P. and SMITH W.H.F. 1998. New, improved version of Generic Mapping Tools released. *EOS, Transaction, American Geophysical Union* 79: 579.
- WILDE-PIÓRKO M., GRAD M., WIEJACZ P. and SCHWEITZER J. 2009. HSPB seismic broadband station in Southern Spitsbergen: First results on crustal and mantle structure from receiver functions and SKS splitting. *Polish Polar Research* 30: 301–316.
- WORSLEY D. 2008. The post–Caledonian development of Svalbard and the western Barents Sea. *Polar Research* 27: 298–317.

Received 18 November 2020

Accepted 14 February 2020